measured and expected values of shear stress near the surface is quite large. A "correction" that increases the vertical wire sensitivity to that necessary to force a correct value for the u-component was applied to both the vertical and yawed wires.[4] The correction (shown as the solid points on Fig. 3) was an improvement in the agreement, but still not adequate. It is not obvious that one could expect the sensitivity of the yawed wire to be affected identically to that of the vertical wire. For the case of the low speed boundary layer,[3] where the turbulence gradients were more important, this form of correction was reasonable. As opposed to the present results, the uncorrected low speed results gave too great a value of $\overline{uv}$ near the wall.

Figure 3 also shows the split film probe measure of the shear stress. The output was evaluated by assuming each film can be treated similar to a yawed hot wire.[5] Attempts to employ the difference or the ratio of the heat transfer from the two films[6] were abandoned, since these functions were found to depend both on flow direction and velocity. The split film results indicate an improvement in the evaluation of $\overline{uv}$ over that of the X-wire. However, the gradient problem is still important near the surface. It is doubtful that the probe size can be further reduced to completely overcome the gradient effects at high speeds.

Conclusions

It is demonstrated that major errors are encountered when mean and turbulent velocity gradients exist along the length of hot wire sensors. Although the problem is also present in low speed measurements it is more pronounced at the high speeds. For the present case evaluated the errors are too great to be corrected accurately. Although the split film sensor results showed a significant improvement over the X-wire sensor results, further reduction in the space resolution of sensors by approximately an order of magnitude would appear to be necessary to reduce the error to acceptable values near the wall.

References

[1] Johnson, D.A. and Rose, W.C., "Laser Velocimeter and Hot-Wire Anemometer Comparison in a Supersonic Boundary Layer," *AIAA Journal*, Vol. 13, April 1975, pp. 512-515.

[2] Sandborn, V.A., "A Review of Turbulence Measurements in Compressible Flow," NASA TM X-62,337, March 1974.

[3] Tielman, H.W. and Sandborn, V.A., "Turbulent Shear Measurements in Large Velocity Gradients," Colorado State Univ. Engineering Report CER67-68HWT-VAS68, 1968, Fort Collins, Colo.

[4] Sandborn, V.A., *Resistance Temperature Transducers*, Metrology Press, Fort Collins, Colo. 1972, p. 294.

[5] Sandborn, V.A. and Seegmiller, H.L., "Evaluation of Mean and Turbulent Velocity Measurements in Subsonic, Accelerated Boundary Layers," NASA TM X-62, 488, Sept, 1975.

[6] Spencer, B.W., and Jones, B.G., "Turbulence Measurements with the Split Film Anemometer Probe," *Proceedings of the Symposium of Turbulence in Liquids*, Univ. of Missouri-Rolla, Rolla, Mo. 1971.

Production of Diamonds from Graphite Using Explosive-Driven Implosions

I.I. Glass* and S.P. Sharma†
University of Toronto, Toronto, Canada

Introduction

NATURAL diamonds have been used by man since antiquity as charms and ornamental objects. Its allotropic form of carbon was established by Tennant in 1797,[1] and led to several attempts to produce it synthetically. However, it was not until 1954 that synthetic diamonds, in the 100- to 1000-μ range, finally were produced at General Electric by Bundy et al.[2] They applied a large hydraulic press ($>$ 50,000 atm) for about 5 min to a graphite cartridge that was heated simultaneously to high temperatures ($>$ 2000° K) by an electric current. Such physical conditions[3] were not attainable before in the laboratory, and this prevented the early experimenters from synthesizing diamonds from carbon. In 1961, diamonds were produced by explosive shock compression and heating of graphite powder in a cartridge.[4] In this case, the pressures of 200 to 300 kbar were applied only for microseconds in order to produce diamond aggregates of 0.05 to 0.1 μ. The foregoing types of processes now are used commercially for producing industrial diamonds suitable for lapping and polishing.

Diamonds also have been produced by using multipoint detonators to initiate a spherical shell of explosive, thereby

Received Nov. 12, 1975. The financial support from the National Research Council of Canada and the U.S. Air Force under Grant No. AF-AFOSR 72-2274C is acknowledged with thanks.

Index categories: Multiphase Flows; Shock Waves and Detonations; Hypervelocity Impact.

*Professor, Institute for Aerospace Studies. Fellow AIAA.

†Research Assistant, Institute for Aerospace Studies.

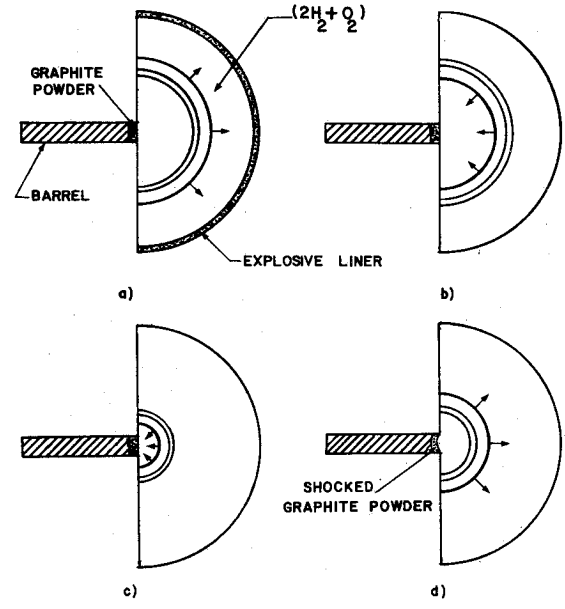

Fig. 1 Operation of UTIAS implosion chamber facility. a) Ignition and outgoing detonation wave. b) Detonation of explosive liner and detonation wave reflection. c) Strong imploding shock wave. d) Imploding shock wave reflection and compression of graphite powder at the origin.

Fig. 2 Scanning electron micrograph of unshocked graphite powder (8400×).

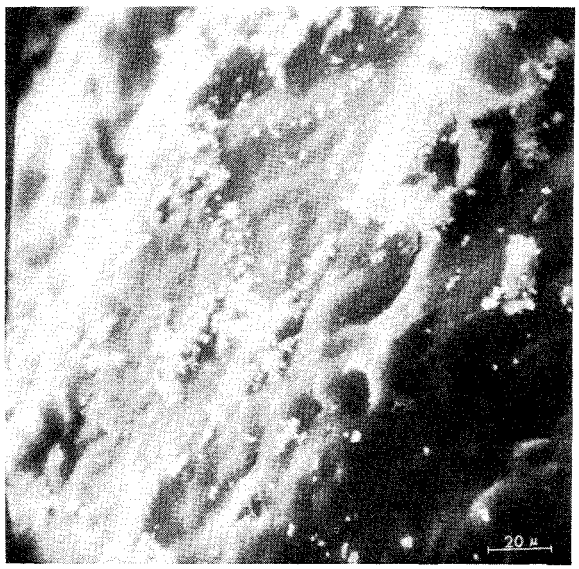

Fig. 3 Scanning electron micrograph of shocked graphite powder (8800×).

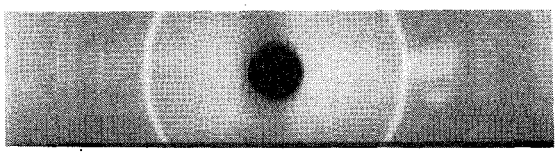

Fig. 4 X-ray diffraction patterns of shocked graphite powder. No diamond reflection line visible.

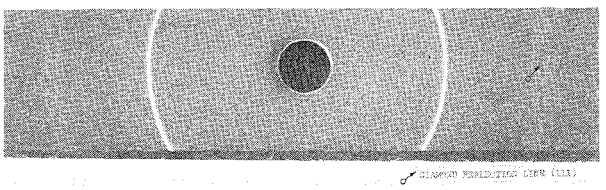

Fig. 5 X-ray diffraction patterns of shocked graphite powder. Only diamond reflection line (111) visible (Cu/ni,15 mA/40 KV, 114.8-mm camera, 2-hr exposure, sample rotated).

generating an implosion, which compressed a spherical piston containing a cartridge of graphite.[5] This method has not been used commercially yet. Another technique utilized an implosive shock wave in an exponentially tapered horn of hardened steel. The initial shock wave was produced by a magnetic hammer. The converging shock hit a graphite cartridge, thereby producing diamonds.[6] Further details can be found in Ref. 7.

Experimental Method

The present method is unique in that it makes use of an apparatus, the UTIAS Implosion Chamber, for the production of micron-size diamonds which was used previously as a driver for hypervelocity projectiles and shock waves.[8-10] The operation is as follows (Fig. 1). A stoichiometric mixture of hydrogen-oxygen is introduced into a hemispherical chamber (20 cm diam), at initial pressures of 27.2 atm, and is detonated by an exploding wire (4 mil diam × 1.25 mm long) located at the geometric center. The spherical detonation wave travels toward the periphery of the chamber, which contains a hemispherical shell of explosive (PETN, about 3 mm thick, 100 g). Ideally, the gaseous detonation instantly and simultaneously detonates the PETN, which sends an implosion toward the geometric center (origin), where a cartridge of graphite is located. The implosion converges on and reflects from the origin, thereby shock-compressing and heating the graphite to produce diamonds. In practice, the initiation and convergence is not always ideal, and the implosion is then off-center, resulting in a dissipation of the implosion energy and therefore a reduced yield of diamonds. Although the calculated pressure, density, and temperature profiles at the origin, as the implosion converges and reflects, are very high, neither they nor those existing in the graphite have been measured. However, the fact that diamonds were produced shows that they meet the requirements of the phase diagram for diamond synthesis.

Results

A number of tests have to be applied in order to confirm that diamonds indeed have been produced. The simplest test is to see if the diamonds will scratch a piece of polished sapphire, which has a hardness of 9 on a Mohs scale compared to diamond. This was achieved readily in this case. Next, the graphite was examined before and after shock compression and heating using a scanning electron microscope. Figure 2 shows a micrograph of unshocked graphite powder at a magnification of 8400-fold. The loose and flaky appearance is quite evident. Figure 3 shows a micrograph of shocked graphite powder at a magnification of 8800-fold. The appearance of spherical globules of about 1 μ diam, many of which are diamond crystals, are seen readily. (The crystal structure of graphite is hexagonal, whereas that of diamond is cubic.) Finally, in order to verify that diamonds actually are present, samples have to be subjected to x-ray diffraction tests. Figure 4 shows a diffraction pattern of not-fully-compressed graphite, where the implosion was off-center, and diamonds therefore were not produced. Figure 5 shows a diffraction record where the diamond reflection line from the (111) face is visible. It is estimated that the yield from the present experiments consisted of about 5% diamonds in the micron-diameter range. Additional details can be found in Ref. 7.

Conclusions

Industrial diamonds have been produced from graphite in a unique manner by using explosive-driven implosions that were used previously to generate hypervelocities of projectiles and shock waves. Although the yield is relatively low, there are possibilities of improvement by perhaps an order of magnitude through further development. The use of the UTIAS Implosion Chamber for the production of synthetic diamonds has important advantages of a safe, controlled, and reusable facility.

References

[1]Tennant, S., "Diamond—An Allotropic Form of Carbon," *Philosophical Transactions*, Vol. 87, Dec. 15, 1796, p. 123.

[2]Bundy, F.P., Hall, H.T., Strong, H.M., and Wentorf, R.H., "Man-Made Diamonds," *Nature*, Vol. 176, No. 4471, July 9, 1955, pp. 51-55.

[3]Bundy, F.P., "Direct Conversion of Graphite to Diamond in Static Pressure Apparatus," *Journal of Chemical Physics*, Vol. 38, Feb. 1963, pp. 631-643.

[4]DeCarli, P.S. and Jamieson, J.C., "Formation of Diamond by Explosive Shock," *Science*, Vol. 133, No. 3467, June 9, 1961, pp. 1821-1822.

[5]Garrett, D.R., "Device for Diamond Synthesis," U.S. Patent 3, 659,072, May 1972.

[6]Rasquin, J.R. and Ester, M.F., "Apparatus for Making Diamonds," U.S. Patent 3,632,242, Jan. 4, 1972.

[7]Sharma, S.P., "Production of Diamonds from Graphite Using Explosive-Driven Implosions," TN 196, 1975, University of Toronto, Institute for Aerospace Studies.

[8]Flagg, R.F. and Glass, I.I., "Explosive-Driven Spherical Implosion Waves," *The Physics of Fluids*, Vol. 11, Oct. 1968, pp. 2282-2284.

[9]Glass, I.I., "Appraisal of UTIAS Implosion-Driven Hypervelocity Launchers and Shock Tubes," *Progress in Aerospace Scien-*

ces, Vol. 13, edited by D.Kuchemann, Pergamon Press, Oxford and New York, 1974, pp. 257-324.

[10]Glass, I.I., Chan, S.K., and Brode, H.L., "Strong Planar Shock Waves Generated by Explosively-Driven Spherical Implosions," *AIAA Journal*, Vol. 12, March 1974, pp. 367-374.

Approximate Calculation of Transient Heat Conduction

Tse-Fou Zien*
Naval Surface Weapons Center, White Oak Laboratory, Silver Spring, Md.

Nomenclature

A	= constant in the given boundary heat flux
a	= constant in the given boundary temperature
f	= temperature profile
HBI	= heat-balance integral
k	= thermal conductivity
n	= exponent
Q	= dimensionless heat flux at $x=0$, Eq. (10)
q	= heat flux
T	= temperature
t	= time
x	= space coordinate
α	= thermal diffusivity
β	= a profile parameter
Γ	= Gamma function
δ	= modified thermal penetration depth
Θ	= dimensionless boundary temperature, Eq. (17)
θ	$= T-T_\infty$

Subscripts

∞	= condition at $x=\infty$ or initial condition
0	= condition at $x=0$

Introduction

THE purpose of this Note is to present a simple, yet accurate, method for solving a variety of transient heat-conduction problems. The method represents a further development of the basic ideas used previously in the approximate calculation of skin friction[1,2] and heat transfer[3] associated with boundary-layer flows. It is an integral approach, and its distinguishing feature lies in the use of an integral expression for the boundary flux. In the application to heat-conduction calculations, the method may be considered as a refinement of the heat-balance integral (HBI) method due to Goodman.[4]

In the present Note, the application of the method is illustrated by solving a class of transient heat-conduction problems in which the surface condition (temperature or heat flux) varies as a power of time. The approximate solutions are compared with corresponding exact solutions as well as the solutions by the HBI method. The accuracy and relative merits of the present method are thus made evident. We note that the method is equally applicable to nonlinear problems of heat conduction, e.g., problems involving phase transitions.

Received October 14, 1975; revision received December 8, 1975. This research was supported by NAVSURFWPNCEN/WOL Independent Research Program.

Index category: Heat Conduction.

*Leader, Fluid Mechanics Group, Experimental Aerodynamics Branch. Associate Fellow AIAA.

Method of Solution

Consider the standard equation of one-dimensional transient heat conduction in a semi-infinite solid,

$$\frac{\partial\theta}{\partial t}=\alpha\frac{\partial^2\theta}{\partial x^2},\quad t>0,\quad 0<x<\infty \tag{1}$$

where, for simplicity, the thermal properties of the solid are assumed constant. An integration of Eq. (1) over the entire region of interest yields the heat-balance integral as

$$\int_0^\infty\frac{\partial\theta}{\partial t}\,dx=\alpha\left(\frac{\partial\theta}{\partial x}\right)_\infty-\alpha\left(\frac{\partial\theta}{\partial x}\right)_0 \tag{2}$$

which, after assuming $(\partial\theta/\partial x)_\infty=0$, reduces to

$$-\alpha\left(\frac{\partial\theta}{\partial x}\right)_0=\int_0^\infty\frac{\partial\theta}{\partial t}\,dx \tag{3}$$

In the usual HBI approach,[4] Eq. (3) is the sole equation for the problem once an approximate temperature profile, $\theta=f(x,t)$ containing one profile parameter, is substituted into Eq. (3). However, in the present treatment, Eq. (3) is used as an expression for the boundary heat flux, $(\partial\theta/\partial x)_0$, and a second equation is to be generated for the determination of the profile parameter.

In the present Note, we choose to generate the second equation by an integration of a moment-like equation. Thus, multiplying Eq. (1) by θ and integrating over the entire domain of interest, we get

$$\int_0^\infty\frac{\partial\theta^2}{\partial t}\,dx=\alpha\left(2\theta\frac{\partial\theta}{\partial x}\right)_\infty-\alpha\left(2\theta\frac{\partial\theta}{\partial x}\right)_0-2\alpha\int_0^\infty\left(\frac{\partial\theta}{\partial x}\right)^2dx \tag{4}$$

With the usual boundary conditions of $\theta_\infty=(\partial\theta/\partial x)_\infty=0$. Eq. (4) reduces to

$$\int_0^\infty\frac{\partial\theta^2}{\partial t}\,dx=-2\alpha\theta_0\left(\frac{\partial\theta}{\partial x}\right)_0-2\alpha\int_0^\infty\left(\frac{\partial\theta}{\partial x}\right)^2dx \tag{5}$$

Equations (3) and (5) form the basis of the solution process when a temperature profile, f, is substituted for θ. For problems where θ_0 is given, the two equations combine to determine the unknowns $(\partial\theta/\partial x)_0$ and the profile parameter. If the surface heat flux is given, a profile containing two parameters will generally be used, and Eqs. (3) and (5) are used to determine the two parameters.

Applications

Power-Law Boundary Temperature

We first consider the case where $\theta_0=at^{n/2}(n\geq 0)$ with $\theta_\infty=0$. An exponential profile will be assumed for the temperature, i.e.,

$$f=at^{n/2}e^{-x/\delta} \tag{6}$$

which satisfies the essential boundary conditions of $\theta_0=at^{n/2}$ and $\theta_\infty=0$. The profile parameter, $\delta(t)$, plays the role of thermal penetration depth but with a slightly modified definition.

Substitution of Eq. (6) into Eqs. (3) and (5) gives the following pair of equations:

$$3\frac{d\delta}{dt}+n\frac{\delta}{t}=2\frac{\alpha}{\delta} \tag{7}$$

and

$$-\left(\frac{\partial\theta}{\partial x}\right)_0=at^{n/2}\left(\frac{n}{2}\frac{\delta}{t}+\frac{d\delta}{dt}\right) \tag{8}$$